Electronics and Electrical Engineering

AIMS Electronics and Electrical Engineering, 3(4): 328–346.
DOI: 10.3934/ElectrEng.2019.4.328
Received: 27 June 2019
Accepted: 15 October 2019
Published: 01 November 2019

http://www.aimspress.com/journal/ElectrEng

Research article

Application of blind source separation to the health monitoring of electrical and mechanical faults in a linear actuator

Ryan Michaud[1], Romain Breuneval[1,3], Emmanuel Boutleux[2,*], Julien Huillery[2], Guy Clerc[1] and Badr Mansouri[3]

[1] Université de Lyon, UCB Lyon 1, CNRS, AMPERE, F-69100, Villeurbanne, France
[2] Université de Lyon, Ecole Centrale LYON, CNRS, AMPERE, F-69130, Ecully, France
[3] Safran Electronics & Defense, Avionics Division, Massy, France

*** Correspondence:** Email: emmanuel.boutleux@ec-lyon.fr; Tel: +33472186094.

Abstract: This paper proposes an automated fault isolation and diagnostic chain for the health monitoring of a linear actuator composed of a roller screw driven by a permanent magnet synchronous motor. Four health conditions are considered and diagnosed: the healthy condition, a short circuit in the stator windings, a mechanical backlash in the roller screw, and the combination of both faults. In order to separate the fault signatures, empirical mode decomposition is applied to the motor current, followed by independent component analysis, automatic isolation of the fault signatures, and a classification step for the diagnosis. The novelty proposed consists of an automatic processing of the independent components to isolate the effects of the short-circuit from the effects of the backlash. This isolation step, in contrast to earlier works, requires no human intervention to select signals of interest, making it suitable to real-time onboard diagnostics. Furthermore, results show that independent component analysis occupies an important role in the diagnosis: its omission leads to a reduction in the diagnostic performance of the classifier as well as a reduction in measures of class separability.

Keywords: electrical actuators; fault detection; health monitoring; blind source separation; empirical mode decomposition; independent component analysis

1. Introduction

The aviation industry is moving toward the replacement of actuators, that were traditionally

hydraulically or pneumatically powered, by electromechanical devices. Operation costs and safety considerations require effective fault diagnosis methods [1–3]. This paper demonstrates the value that Independent Component Analysis (ICA) can bring to a fault detection signal processing chain for an electromechanical actuator. Two separate faults are simulated independently: a short circuit on one of the phases of the synchronous electric motor, and backlash in a roller screw. A third fault is the simultaneous combination of short circuit and backlash.

ICA is a signal processing technique that is part of a larger family of methods called Blind Source Separation (BSS) [4]. BSS can be used when several different source signals are mixed together in the observations. The goal of BSS is to process these observations to separate the original source signals. The separation is blind because the separation procedure uses weak a priori assumptions about the sources and the mixing parameters. ICA is a specific type of BSS that bases its separation procedure on the assumption that the sources are independent. Electro-mechanical systems are an example of systems where such source mixing can occur. The mixing of such signals renders fault diagnosis more difficult because different fault signatures are mixed together between themselves and with other nominal operating signals. In this application for example, the effects of a short circuit are mixed with backlash effects, which are in turn both mixed with the nominal effects of load and reference signal. In this case, the goal of ICA would be to help to separate the fault signatures to ease the diagnosis process.

In its basic version, ICA requires the same number of measurements as sources. In this work, it is desirable to use only a single measurement, the motor current I_q, as the basis for the diagnosis. The reasons for this are primarily economic: the motor current I_q is already measured for the field-oriented control of the electric motor. Applying ICA to a single-channel recording has been addressed by researchers in the past. The approaches consist of first decomposing the single-channel measurement into a series of different spectral modes before then applying ICA. An approach entitled wavelet-ICA is used in [5]. The authors use a wavelet transform to decompose a single-channel signal into several signals upon which ICA is applied. A disadvantage of this method is that the user must parameterize the mother wavelet and that non-stationary fault features that span across several wavelet coefficients cannot be handled. In an alternate approach developed in [6] and [7], the signal decomposition is done by an Empirical Mode Decomposition (EMD). EMD has the advantage of being a data-driven decomposition as no initial parameterization is required and it can naturally handle non-stationary signals. However, the two methods proposed above require manual user intervention: once a set of independent components are identified by ICA, a subset of these are manually chosen as "signals of interest" and recombined to create an estimate of the desired signal. In this paper, an automatic selection of the independent components is proposed, which allows the isolation of the fault signatures without manual intervention.

This paper is organized as follows: section 2 describes the physical system and the simulation model. Section 3 is dedicated to ICA, which is the main component of this paper. Section 4 describes the data processing chain, including the steps before and after ICA. The pre-processing uses EMD and the post-processing is accomplished with the proposed automatic isolation method. Section 5 presents fault diagnosis results from a basic classifier and highlights the advantages of using the ICA step.

2. System description

The application relates to an electro-mechanical actuator illustrated in Figure 1. A permanent magnet synchronous motor (PMSM) rotates a roller screw drive, which actuates a mass subjected to

an external load. Three faults are considered here: a partial short-circuit on one of the motor's stator windings, an abnormal mechanical backlash [8–10] in the roller screw drive and the simultaneous combination of both faults.

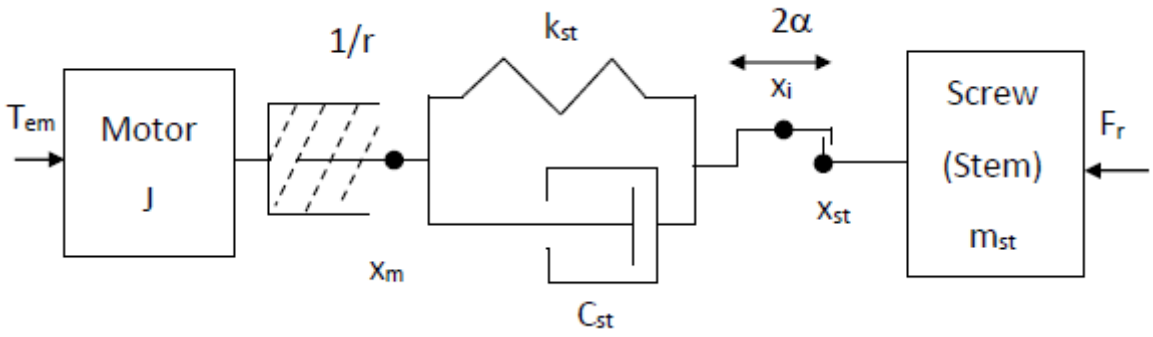

Figure 1. Schematic of electro-mechanical actuator.

2.1. Electromechanical model

The non-linear model of the system includes the effects of stem deformation and backlash in the roller screw [11,12]. The model was adapted from [13] and described in [14].

2.1.1. Dynamics of the roller screw system

Let x_m represent the motor's equivalent linear position, x_i the intermediate position, x_{st} the stem position, k_{st} the stem stiffness, c_{st} the damping ratio of the stem and 2α the backlash gap. The following variables can then be defined:

$$\begin{aligned} x_d &= x_m - x_{st}: \textit{the gap between positions} \\ x_b &= x_i - x_{st}: \textit{the backlash position} \\ x_s &= x_m - x_i: \textit{the stem deformation} \end{aligned} \tag{1}$$

Then the deformation force F_s, which makes the link between the motor and the stem, can be calculated by:

$$F_s = F_{kst} + F_{cst} = k_{st}(x_s - x_{s0}) + c_{st}\dot{x}_s \tag{2}$$

Three cases can be identified to define the dynamics of x_b:
Left contact ($x_b = -\alpha$ and $F_s \neq 0$):

$$\dot{x}_b = \max\left[0\,;\, \dot{x}_d + \frac{k_{st}}{c_{st}}(x_d - x_b - x_{s0})\right] \tag{3}$$

Right contact ($x_b = +\alpha$ and $F_s \neq 0$):

$$\dot{x}_b = \min\left[0\,;\, \dot{x}_d + \frac{k_{st}}{c_{st}}(x_d - x_b - x_{s0})\right] \tag{4}$$

No contact (Backlash) ($|x_b| < \alpha$ and $F_s = 0$):

$$\dot{x}_b = \dot{x}_d + \frac{k_{st}}{c_{st}}(x_d - x_b - x_{s0}) \tag{5}$$

Then Newton's second law is applied to the stem:

$$m_{st}\ddot{x}_{st} = F_s - F_f - F_r \tag{6}$$

with m_{st}: the mass of the stem and of the connected elements; F_f: the friction forces; F_r: the load force and the initial deformation x_{s0}.

The friction model, which is proposed here, comes from [15]:

$$F_f = F_v\dot{x}_{st} + sign(\dot{x}_{st})[F_d + K_l.abs(F_r)] \tag{7}$$

with F_f: the friction force (N); $\dot{x}_{st}$: the stem speed (m/s); F_v: the viscous friction parameter (N/(m/s)); $sign$: the sign function; F_d: the dry friction parameter (N); K_l: the load friction parameter; abs: the absolute value function.

2.1.2. Dynamic model of PMSM rotor

The connection to the rotor is made by:

$$J\dot{\Omega} = T_{em} - T_s = T_{em} - \frac{F_s}{r} \tag{8}$$

with $r = \frac{2\pi}{l}$, l: the roller screw thread pitch (m), J: the rotor inertia (kg.m²), Ω: rotor's speed (rad/s) and T_{em}: the motor torque given by

$$T_{em} = p\Psi_M I_q \tag{9}$$

with p: the number of pole pairs; Ψ_M: the magnetic flux of the permanent magnets; I_q: the current in the quadrature axis of Park's frame.

I_d and I_q currents are given by a fine-resolution simulation of the drive. The model of the electro-mechanical actuator includes

- the roller screw which is supposed to be the main source of friction
- the non-salient poles PMSM model
- a vector control part

This model has been identified and validated on an experimental bench [16].

The PMSM model is obtained in a modified four axis rotor reference frame. An inter-turn fault in the phase is also embedded in the model. It is represented by an auxiliary winding loaded by a resistance Rf. As shown in Figure 2, the faulty PMSM is composed of four coils supplied respectively by four currents i_a, i_b, i_c, i_f. The number of turns of the auxiliary winding and the Resistance Rf can be adjusted. Thus the number of short-circuited turns and the severity of the fault can be adjusted in simulation [17].

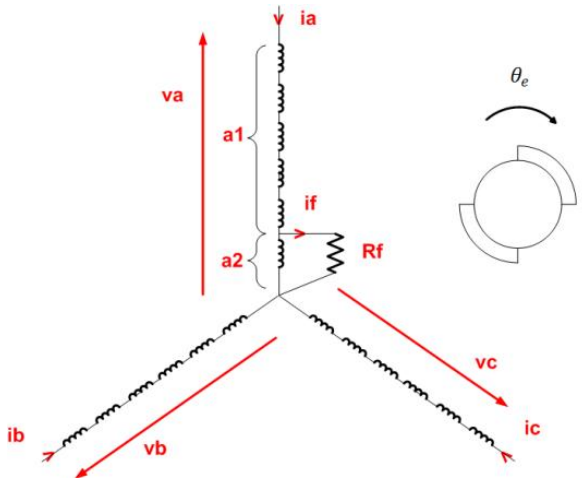

Figure 2. The external model of a faulty machine**.**

2.2. Position control model

In addition to the dynamic model of the roller screw and motor described above, the simulation model includes a position control system as illustrated in the block diagram of Figure 3. The position/speed control is a cascade PI control. The current control uses an RST controller.

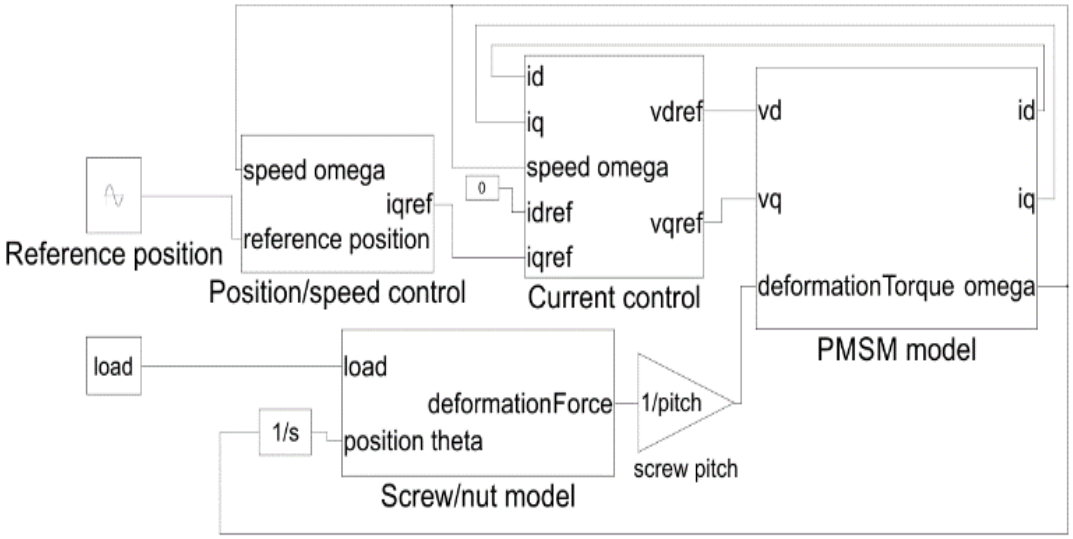

Figure 3. Block diagram of simulation model, including position control loop.

2.3. Effects of faults on the motor currents

As can be seen in Figure 3, the I_d and I_q motor currents are measured as part of the control system. The I_q motor current is chosen for the diagnostic because it is more sensitive to the fault conditions. The short circuit adds a high frequency oscillation over the healthy waveform as shown in Figure 4. The zoom shows that a small high frequency component is already present in the healthy condition. As shown in Figure 5, the backlash introduces a delay and amplifies the spike in the current. The presence of both faults causes high frequency oscillations and spikes as shown in Figure 6.

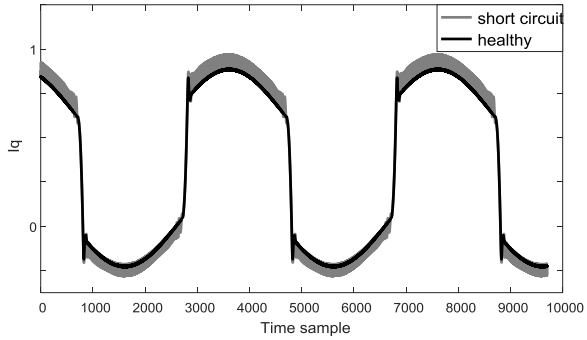

Figure 4. Effect of short circuit on current $\boldsymbol{I_q}$.

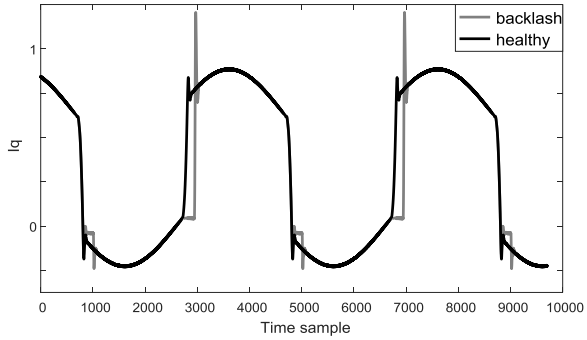

Figure 5. Effect of backlash on current $\boldsymbol{I_q}$.

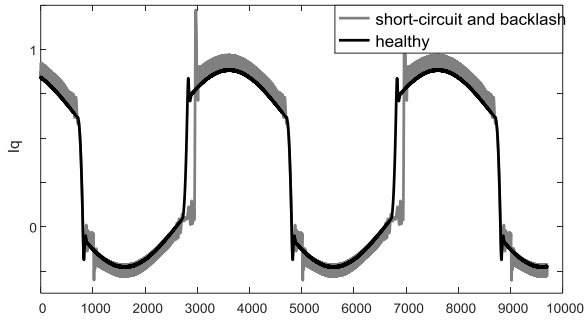

Figure 6. Effect of both faults on current $\boldsymbol{I_q}$.

3. Independent component analysis (ICA)

3.1. ICA problem definition

In its basic form, ICA supposes that a set of m random variables $x_1, \dots, x_m$, is observed, which are linear combinations of n random source variables $s_1, \dots, s_n$:

$$x_i = a_{i1}s_1 + a_{i2}s_2 + \cdots + a_{in}s_n, \quad i = 1, \dots, m \tag{10}$$

Or alternatively, in vector-matrix notation:

$$\mathbf{x} = \mathbf{As} \tag{11}$$

where $\mathbf{x} = [x_1, \dots, x_m]^{\mathrm{T}} \in \mathbb{R}^m$ is the random observation vector, $\mathbf{s} = [s_1, \dots, s_n]^{\mathrm{T}} \in \mathbb{R}^n$ is the random source vector and $\mathbf{A} \in \mathbb{R}^{\mathrm{m}\times\mathrm{n}}$ is the mixing matrix whose coefficient entries $a_{ij}, i = 1, \dots, m; j = 1, \dots, n$ define the linear combination of the source vectors.

ICA seeks to find a matrix $\mathbf{W} \in \mathbb{R}^{\mathrm{n}\times\mathrm{m}}$ that enables an estimate $\hat{\boldsymbol{s}}$ of the source vector to be obtained from the observations:

$$\hat{\mathbf{s}} = \mathbf{W}\mathbf{x} \tag{12}$$

It has been shown in [18] that estimates for **s** and **W** can be found if the two following conditions are met:

- the source variables are statistically independent,
- at most one of the source variables has a Gaussian distribution.

An additional condition that is usually assumed is that the number of sources and observations is the same, that is $m = n$. Although this is not a strict requirement as approaches for under or over-determined mixtures exist (see for example in [19] or [20]), the separation problem becomes much more complex. The ICA procedure employed here assumes the same number of sources as observations.

3.2. ICA implementation

One of the central problems in ICA is the difficulty in directly measuring the statistical independence. By definition, a set of arbitrary random variables $\mathrm{y}_1, \dots, \mathrm{y}_\mathrm{n}$, are independent if their joint probability density function can be expressed as the product of the marginal probability density functions:

$$p(y_1, y_2, \dots, y_n) = p(y_1)p(y_2) \dots p(y_n) \tag{13}$$

In practice, this definition is not useful because it is very difficult to estimate these distributions. ICA procedures must therefore rely on alternate measures of independence. Once an independence measure is chosen, ICA becomes an optimization problem to find the unmixing matrix W which maximizes the independence measure of the estimated sources.

For this work, a well-known and computationally efficient algorithm of ICA entitled FastICA is used. In this algorithm, the statistical independence is maximized by maximizing the non-gaussianity of prewhitened data. This algorithm is presented in [4] and [21] and available for download at [22].

4. Signal processing chain

This section describes the different steps which have been involved in the signal processing chain. According to (11) x_{I_q} is the observation of current I_q (i.e. the measured current). As shown in Figure 7, the measured current x_{I_q} is first decomposed, by Empirical Mode Decomposition (EMD), into a set of signals upon which ICA is applied. The independent components (ICs) that result are then automatically combined in an isolation step to form the estimates of the short circuit ($\hat{\mathrm{s}}_{\mathrm{cct}}$), backlash ($\hat{\mathrm{s}}_{\mathrm{back}}$), and the nominal operation ($\hat{\mathrm{s}}_{\mathrm{nom}}$). In this section, the decomposition method is presented, as well as the parameters used in the FastICA algorithm and the automatic isolation method.

4.1. Pre-processing by complete ensemble empirical mode decomposition with adaptive noise (CEEMDAN)

Since only one observation (the current x_{I_q}) is used, and there are at least three sources in the system (the short circuit, the backlash, and the nominal operation), pre-processing of the single-channel signal x_{I_q} is required to split it into a number of virtual observations that can be processed by ICA.

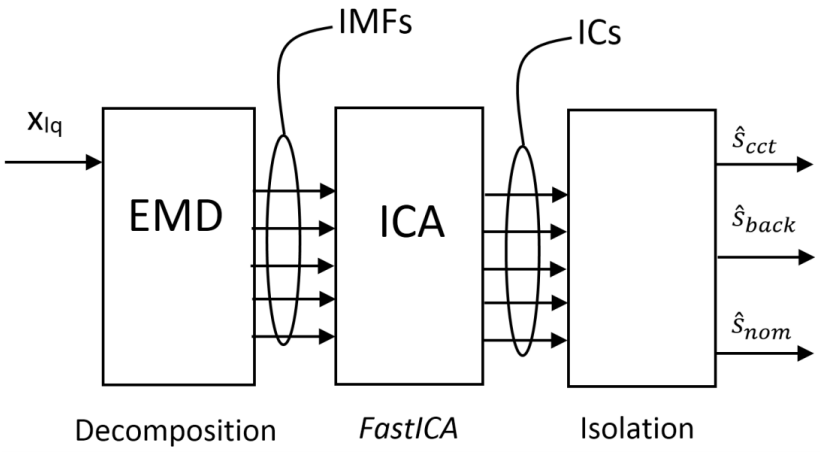

Figure 7. General signal processing scheme.

The choice was made to decompose the single channel current by using the CEEMDAN (Complete Ensemble Empirical Mode Decomposition with Adaptive Noise) procedure presented in [23]. This particular decomposition procedure is a robust extension preventing mode mixing of the basic EMD originally presented in [24]. The result of an EMD is the decomposition of a non-stationary and/or non-linear time series into a set of oscillatory functions called Intrinsic Mode Functions (IMF), or simply "modes". An IMF has two properties:

- The number of extrema and the number of zero crossings are equal or differ at most by one
- The local mean of the upper and lower envelope is zero everywhere [24].

Applying an EMD to an arbitrary signal y gives a decomposition of the form:

$$y = \sum_{j=1}^{k} IMF_j + r_k \tag{14}$$

where r_k represents the final residual, a signal from which no further IMFs can be extracted. The CEEMDAN package developed in the context of [23] was used. It is publicly available at http://perso.ens-lyon.fr/patrick.flandrin/emd.html. The noise standard deviation was set to Nstd = 0.2. The number of noise realizations was set to NR = 100, and the iteration limit was set to MaxIter = 5000.

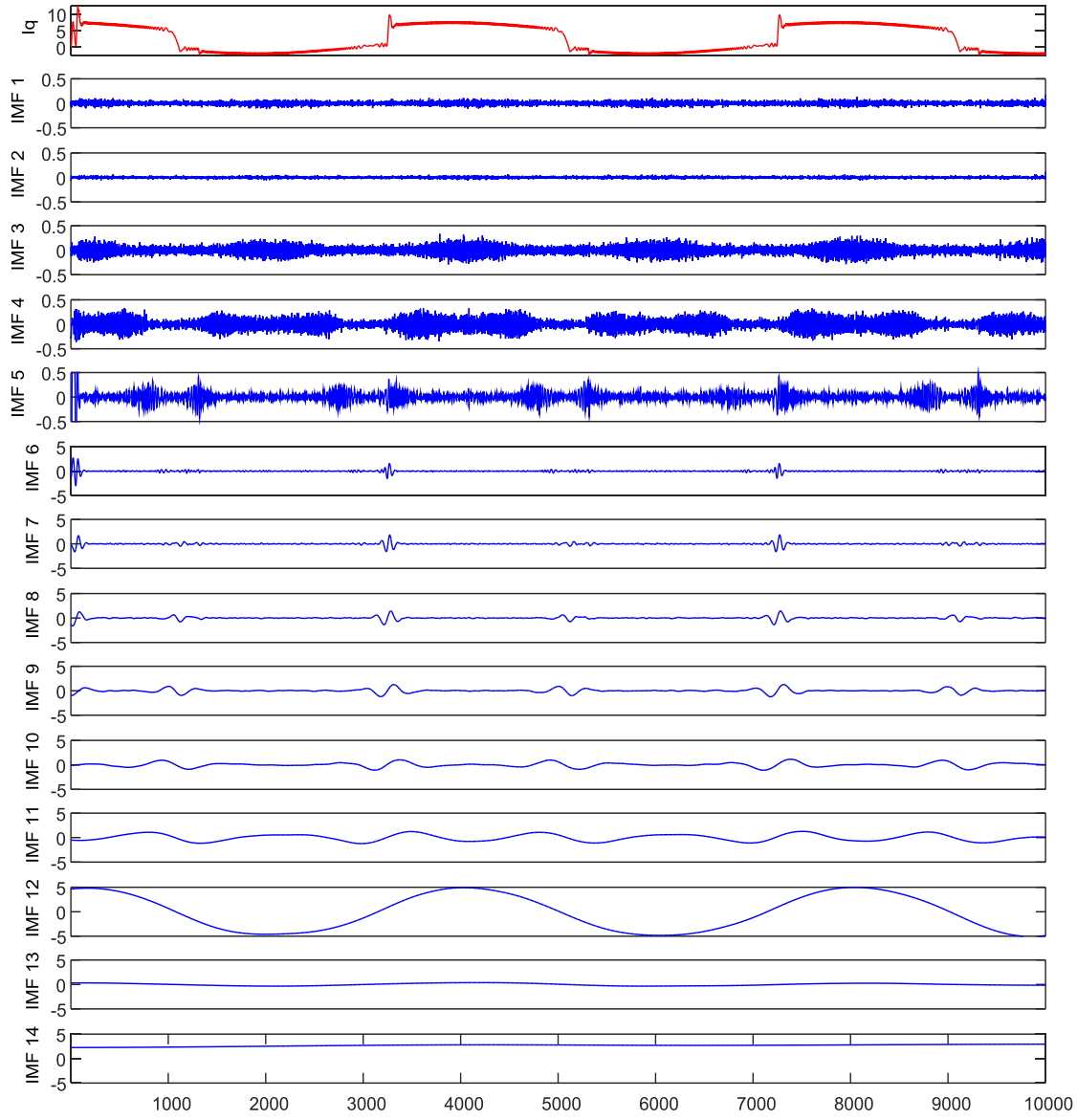

Figure 8. Example of EMD results. The original signal is at the top, the IMFs are below it.

Figure 8 shows an example of the CEEMDAN results. The first graph shows the original signal from which fourteen IMFs were extracted. IMF_1 is below the first graph and IMF_{14} is at the bottom. As illustrated, the order of IMF extraction is from high frequency to low frequency. As the two separate fault conditions both introduce high frequency components in the measured signal, the four last IMFs can be discarded as they do not contain any useful information regarding fault isolation. The signal processing chain of Figure 7 is thus slightly modified as shown in Figure 9, only the first 10 IMFs are conserved for further processing.

4.2. ICA parameters

For the ICA step, the FastICA package [22] was used with the following parameters: non-linearity 'g' = 'gauss', 'stabilization'= 'on', 'epsilon' = 1e-6, 'approach' = 'defl'. When running FastICA on a batch of simulations, a first mixing matrix $\mathbf{A_{init}}$ is found from one of the

simulations. The remaining FastICA separations for the other simulations are initialized to $\mathbf{A_{init}}$ using the 'Aguess' parameter. Example results of the ICA step applied to the first 10 IMFs of Figure 8 are given in Figure 10.

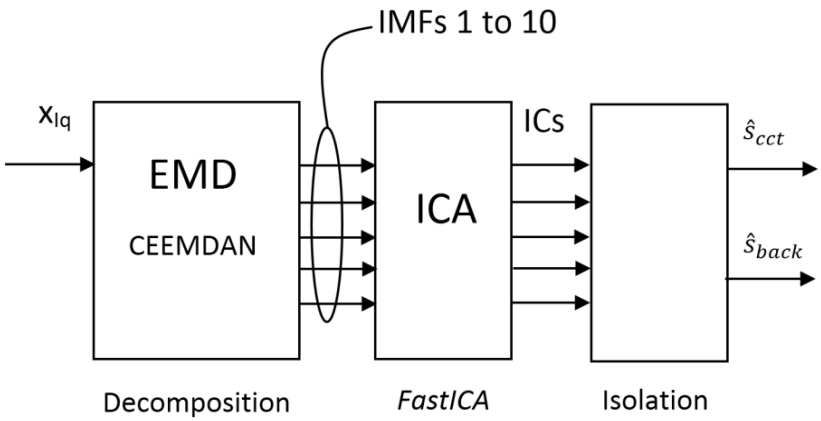

Figure 9. Modified processing chain. Only the first 10 IMFs are passed to the ICA step.

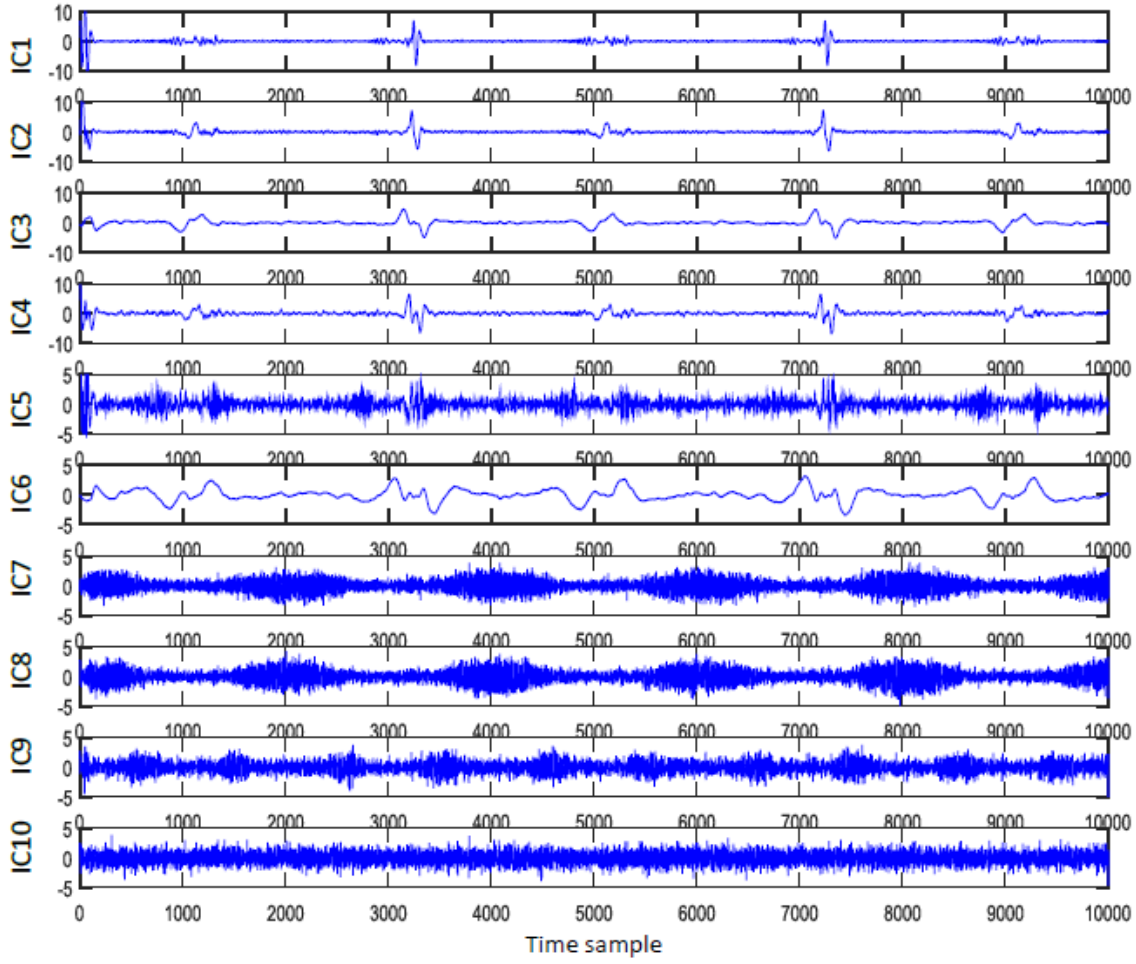

Figure 10. Example ICs resulting from FastICA applied to the IMFs 1 to 10 shown in Figure 8.

4.3. Isolation

The ICA step provides independent components, as shown in Figure 10, but the procedure also provides the estimated mixing matrix A, that defines the linear mapping between the source signals s and the observations x, as in x = As (11). The isolation step involves choosing different subsets of ICs which are multiplied by the estimated mixing matrix A to generate the appearance of the sources in the IMF space. These signals are then summed together, to obtain a single signal that represents a fault signal.

In this application, it was seen that the short circuit fault causes high frequency oscillations and the backlash fault causes spikes in the current (see Figure 4 to Figure 6). The fault signatures step then consists in first selecting a subset of ICs that are mainly oscillatory and another subset that are mainly spiky. A given subset is multiplied by the estimated mixing matrix A, and the resulting signals are summed to obtain the respective source signals.

4.3.1. Automatic subset creation

The general isolation process described above is used in [6] and [7], but no method for automatic subset creation is given and without such an automatic rule, the selection must be done manually. An automatic subset creation process based on kurtosis is presented here.

Knowing that the backlash creates spiky components and the short-circuit creates high-frequency oscillations, kurtosis is used to characterize the spikiness of the ICs. The kurtosis is a statistical measure that represents the normalized fourth central moment. The kurtosis of an arbitrary random variable y is given by:

$$Kurtosis = \frac{\mathbb{E}(y-\mu)^4}{\sigma^4} \tag{15}$$

where $\mathbb{E}(\cdot)$ is the expectation operator, μ is the mean of y, and σ is its standard deviation. In this form, the kurtosis of the Gaussian distribution is 3. The kurtosis measure is commonly used in machine monitoring applications where a faulty component will generate spikes. In monitoring bearings for example, the acceleration signal of a healthy bearing will have a kurtosis value of 3. As the bearing degrades, its acceleration signal will become more spiky and its kurtosis value will become larger than 3 [25].

The kurtosis measure is used to create two subsets of the ICs: the single IC that has the greatest kurtosis value is assigned to the $\hat{s}_{back}$ subset, and the remaining 9 ICs are assigned to the $\hat{s}_{cct}$ subset. The automatic subset creation, and the rest of the isolation process is summarized in Figure 11.

Figure 12 shows an example of $\hat{s}_{back}$ in two conditions: healthy condition in black, and double fault (short circuit plus backlash) condition in grey. Note that even in healthy conditions, small spikes are present, as it can be seen in the healthy curves of Figure 4 to Figure 6. One can notice that the spikes in the double fault signal (grey) are more pronounced due to the presence of the backlash fault. But also of importance is the fact that even though a short circuit is also present, the grey signal is not much more oscillatory than the black signal. The signal processing chain has therefore isolated the impulsive phenomena in $\hat{s}_{back}$.

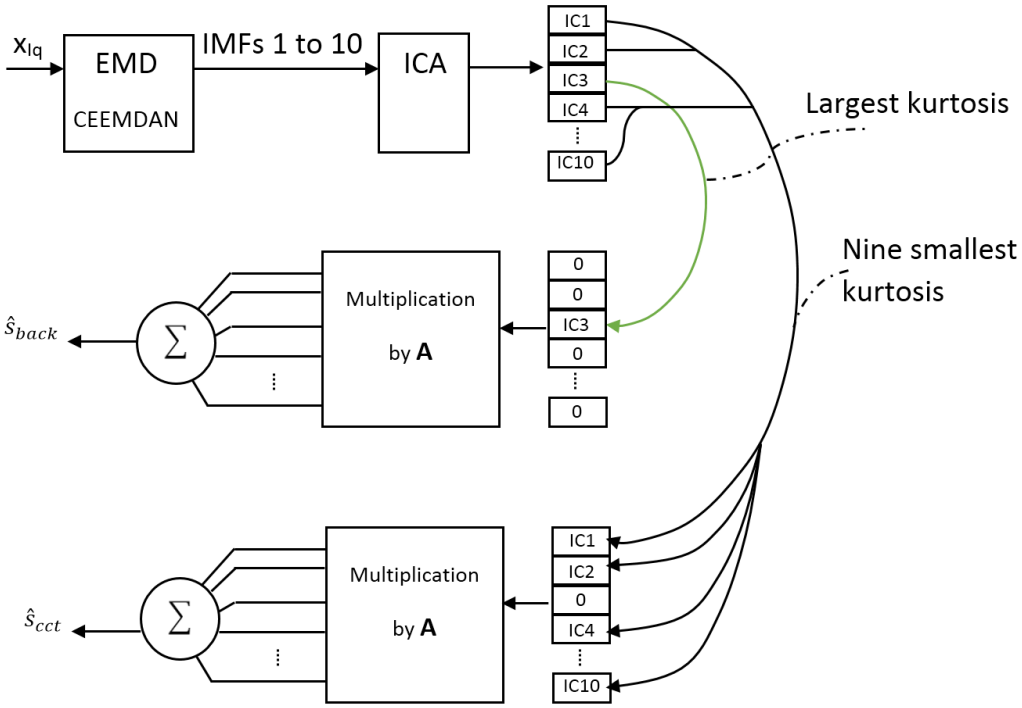

Figure 11. Kurtosis-based automatic isolation.

A similar observation can be made of Figure 13, which shows examples of $\hat{s}_{cct}$ for healthy (black) and double fault (grey) conditions. Note that even in healthy conditions, the current contains oscillations as shown in zoom of Figure 4. The grey signal of Figure 13 has oscillations that are more pronounced due to the presence of the short circuit, but the presence of the backlash does not make $\hat{s}_{cct}$ significantly spikier. Qualitatively, the processing chain has separated the oscillatory and impulsive natures of the current signal. The next section will present an automatic diagnosis procedure applied to these signals.

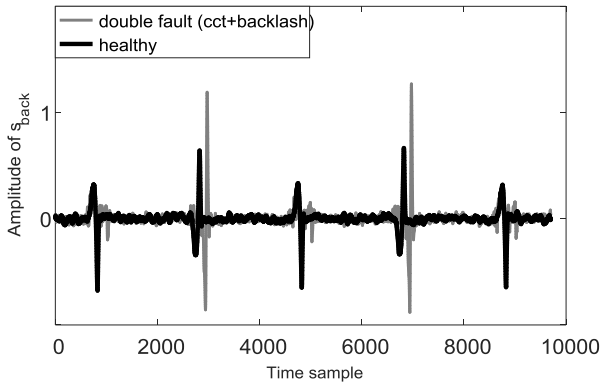

Figure 12. Example of $\hat{s}_{back}$ in healthy (black) and double fault condition (grey).

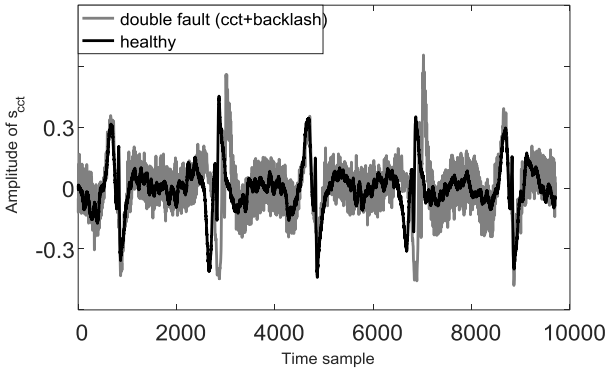

Figure 13. Example of $\hat{s}_{cct}$ in healthy (black) and double fault condition (grey).

5. Fault diagnosis and results

Based on the signals $\hat{s}_{cct}$ and $\hat{s}_{back}$, the system behavior must be assigned to one of four possible classes (Ω_1 to Ω_4): healthy, short circuit only, backlash only, or short circuit plus backlash. The aim here is not to propose a new approach for classification. On the contrary, to highlight the discrimination power of the signal processing approach, a simple k-nearest-neighbor (kNN) decision scheme is employed and cross-validation results are presented. The effects of omitting the ICA step are investigated by leave-one-out cross-validation and scatter-matrix separability criteria.

5.1. Feature extraction

Using the $\hat{s}_{cct}$ and $\hat{s}_{back}$ signals, two features are extracted that are used in the kNN classifier. To characterize the oscillatory nature of $\hat{s}_{cct}$, the number of zero crossings are counted. To avoid the effects of noise, a zero crossing is only taken into account if the change in amplitude between two samples at the zero crossing exceeds a certain threshold. To characterize the spikiness of $\hat{s}_{back}$, a composite feature was created that is called here the "spike factor" defined by:

$$Spike\ factor = number\ of\ spikes \times max\ spike\ amplitude. \quad (16)$$

Here also, the absolute value of a spike must exceed a pre-defined threshold to be taken into account. A value of 1 was found to provide good discriminatory capacity.

5.2. Classifier parameters

Suppose a set of training data that is made up of several observations for which all the feature values and the associated classes are known. Given a new observation for which the class is not known, a k-nearest-neighbor classifier will search the feature space for the k nearest neighbors of the new observation. By majority voting, the new observation will be assigned to the class that is most represented among the k nearest neighbors. A value of $k = 5$ was chosen in this work.

To measure the distance between a new observation and the observations in the training set, the Mahalanobis distance between two points y1 and y2 is used, which takes into account the natural distributions of the observations:

$$d_{Mah}(y_1, y_2) = \sqrt{(y_1 - y_2)\mathbf{C}^T(y_1 - y_2)} \quad (17)$$

where $\mathbf{C}$ is the covariance matrix of the observations. An inverse weighting is also applied on the neighbors such that the closer neighbors have a greater weight in the voting scheme.

5.3. Leave-one-out cross-validation

Given a set of training data, cross-validation can be used to evaluate the performance of the classifier. This consists in dividing the training data in two subsets: one subset that maintains its role as training data, and the second subset that is used as test data. Using the classifier rules and the training subset, the test data is classified. By comparing the classification results to the true known classes of the test subset, a percentage of correctly classified observations can be determined. This cross-validation can be repeated by cycling through the training data and using different parts for the training subset and the test subset. When the test subset consists of a single observation, and the cross-validation is repeated such that each observation in the training data is tested once, the method is called leave-one-out cross-validation.

5.4. Simulations and results with ICA step

For each of the four fault conditions, eight different mechanical loads on the system were simulated, from –100% to +100% of the nominal load, resulting in 32 simulations. The signal processing chain was applied to these 32 simulations and the features were extracted from the $\hat{s}_{cct}$ and the $\hat{s}_{back}$ fault signatures. The kNN classifier and cross-validation were implemented with the Statistics and Machine Learning toolbox from Matlab. Leave-one-out cross validation yielded a classification performance of 93.8%.

5.5. Omitting the ICA step

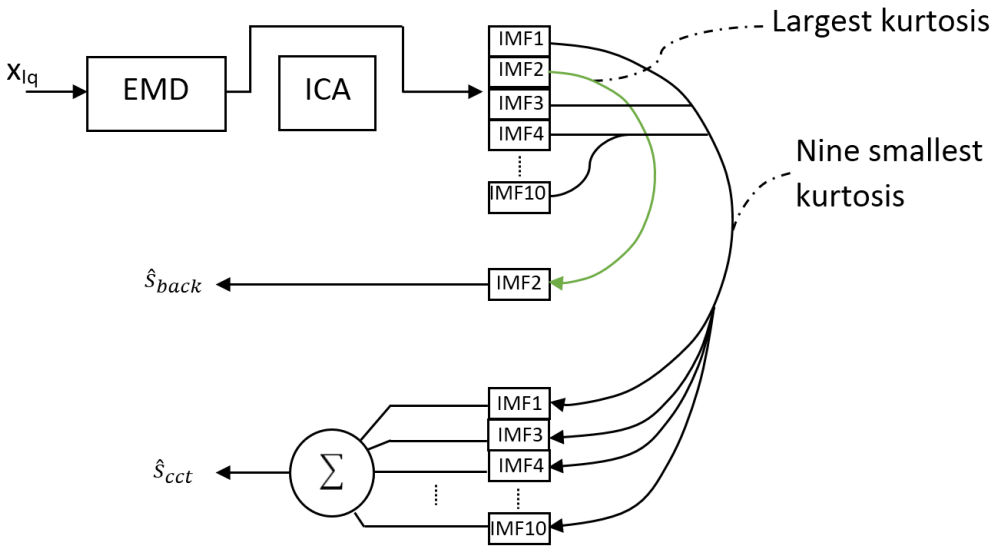

Figure 14. Processing chain without ICA step.

A classification performance of 93.8% is an encouraging result, but does the ICA in the signal processing chain offer a real benefit? Could CEEMDAN alone offer enough separation capacity to allow for an accurate fault diagnosis? This section presents results obtained with a modified signal processing chain omitting the ICA as illustrated in Figure 14. To automatically create the IMF subsets, the same rule as the ICA case is used: the component with the largest kurtosis value is taken as $\hat{s}_{back}$ and the other nine are summed to create $\hat{s}_{cct}$.

By omitting the ICA step, the classification performance dropped by more than fifteen percent, as summarized in Table 1.

Table 1. Cross-validation results (leave one out).

CEEMDAN alone	CEEMDAN + ICA
78.1%	93.8%

5.6. Comparison of separability criteria with and without ICA

The above results show the value of ICA in the proposed fault diagnostic chain with a set of specific parameter choices: $k = 5$ for the kNN rule, the Mahalanobis distance with inverse weighting, the specific choice of features that were extracted related to the zero crossings and the spikes. Several other choices could have been made for each of these parameters. To generalize the results, tests were performed with a larger number of features and class separability criteria based on scatter matrices were used to compare the results obtained with or without the ICA step.

5.6.1. Separability criterium

In general, the aim is to choose features that make classes compact and far apart from one another. In other words, the within-class scatter should be small, and the between-class scatter should be large. The within-class scatter matrix Σ_w, is given by:

$$\Sigma_W = \frac{1}{N}\sum_{i=1}^{M}\sum_{j=1}^{n_i}(x_{ij} - g_i)\cdot(x_{ij} - g_i)^T \tag{18}$$

and the between-class scatter matrix Σ_b is given by:

$$\Sigma_B = \sum_{i=1}^{M}(g_i - g)\cdot(g_i - g)^T \tag{19}$$

where

- g is the center of gravity of the set of observations
- g_i is the center of gravity of class Ω_i
- M is the number of classes
- x_{ij} is the j_{th} observation of class Ω_i
- n_i is the number of observations in class Ω_i
- N is the total number of observations

A scalar criterion J can then be used to compare the relative separability of a set of observations. It involves the determinant of the scatter matrices:

$$J = \frac{\det(\Sigma_w + \Sigma_b)}{\det(\Sigma_w)} \tag{20}$$

5.6.2. Feature selection

Then, an attempt was made to increase the number of components of the pattern vector to improve the classification. Given a large set of features, feature selection techniques attempt to reduce the number of features used while maintaining good class separability. The feature selection method called Sequential Backward Selection (SBS) was used [26]. The technique starts with a full set of features and sequentially removes the feature that penalizes the separability criteria the least until the desired number of features remain.

Eleven different features were chosen for the full set, as listed in Table 2.

Table 2. Features used in SBS.

Features based on $\hat{s}_{back}$
Kurtosis, crest factor, energy, RMS, number of spikes, max peak-to-peak of spikes, spike factor
Features based on $\hat{s}_{cct}$
Energy, RMS, zero crossings
General parameters
Load value

5.6.3. Comparison

The SBS procedure was repeated for subset sizes from 11 to 1. For each subset, the separation criteria value (20) was evaluated for both signal processing chains. Figure 15 shows the results: even for a large number of different feature combinations, the CEEMDAN-ICA allows for a much better separability of the classes. These results suggest that ICA can help to improve the fault diagnostics of the electro-mechanical actuator.

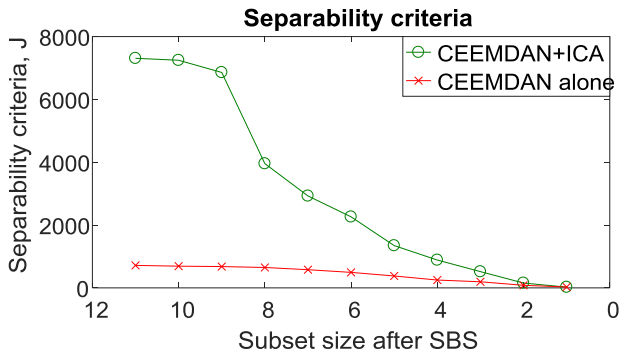

Figure 15. Comparison of separability criteria.

6. Conclusion

A method was presented for automatically isolating fault signatures of a linear actuator made of permanent magnet synchronous motor with roller screw. The signal processing chain is made up of empirical mode decomposition followed by independent component analysis. A novel isolation step based on kurtosis values allows automatic isolation of the fault signatures without manual intervention. The specific value of independent component analysis (ICA) in this chain was shown though degraded performance and separability criteria when ICA was omitted.

7. Glossary

ICA	Independent Component Analysis
BSS	Blind Source Separation
I_q	The motor current in the quadrature axis of Park's frame
EMD	Empirical Mode Decomposition
PMSM	Permanent Magnet Synchronous Motor
A	Mixing matrix
W	Unmixing matrix which maximizes estimated sources independence measure
x_{I_q}	The observation of current I_q ; single measured current used for diagnosis
ICs	Independent Components
$\hat{s}_{cct}$	Estimate of the short circuit
$\hat{s}_{back}$	Estimate of the backlash
$\hat{s}_{nom}$	Estimate of the nominal operation
CEEMDAN	Complete Ensemble Empirical Mode Decomposition with Adaptive Noise
IMF	Intrinsic Mode Functions
Kurtosis	Statistical measure that represents the normalized fourth central moment
SBS	Sequential Backward Selection

Conflict of interest

The authors declare that there is no conflict of interest in this paper.

References

1. Zong W, Wan F, Wei Y (2017) Real-time monitoring for the actuator mechanism of the aileron. *IEEE Prognostics and System Health Management Conference (PHM-Harbin)* 2017: 1–5.
2. Di Rito G, Schettini F, Galatolo R (2018) Model-Based Prognostic Health-Management Algorithms for the Freeplay Identification in Electromechanical Flight Control Actuators. *5th IEEE International Workshop on Metrology for AeroSpace (MetroAeroSpace)*, 340–345.

3. Breuneval R, Clerc G, Nahid-Mobarakeh B, et al. (2017) Hybrid diagnosis of intern-turn short-circuit for aircraft applications using SVM-MBF. *IEEE International Conference on Fuzzy Systems (FUZZ-IEEE)*, 1–6.
4. Hyvärinen A, Karhunen J, Oja E (2001) Independent Component Analysis. 1st ed. New York: Wiley-Interscience.
5. Lin J and Zhang A (2005) Fault feature separation using wavelet-ICA filter. *NDT & E International* 38: 421–427.
6. Mijović B, De Vos M, Gligorijević I, et al. (2010) Source Separation From Single-Channel Recordings by Combining Empirical-Mode Decomposition and Independent Component Analysis. *IEEE T Bio-Med Eng* 57: 2188–2196.
7. Xing H and Hou J (2009) A Noise Elimination Method for ECG Signals. *2009 3rd International Conference on Bioinformatics and Biomedical Engineering*, 1–3.
8. Papageorgiou D, Blanke M, Niemann HH, et al. (2019) Robust Backlash Estimation for Industrial Drive-Train Systems—Theory and Validation. *IEEE T Contr Syst T*.
9. Chen C, Liu Z, Zhang Y, et al. (2016) Actuator Backlash Compensation and Accurate Parameter Estimation for Active Vibration Isolation System. *IEEE T Ind Electron* 63: 1643–1654.
10. Mansouri B, Piaton J, Guyamier A (2016) The backlash gap size estimation for electromechanical actuator in an operational behavior. PHME.
11. Fedotov O, Zhdanov A, Morozov V (2018) Experimental Determination of Kinematic Error for Actuators with Roller-Screw Mechanism. *IEEE International Russian Automation Conference (RusAutoCon)*, 1–5.
12. Zheng S, Fu Y, Zhang Z, et al. (2018) Research on Detect Method for Transmission Accuracy and Efficiency of Planetary Roller Screw Pair. *IEEE International Conference on Mechatronics and Automation (ICMA)*, 1400–1404.
13. Lagerberg A and Egardt B (2007) Backlash estimation with application to automotive powertrains. *IEEE T Contr Syst T* 15: 483–493.
14. Breuneval R, Clerc G, Nahid-Mobarakeh B, et al. (2016) Identification of a roller screw for diagnosis of flight control actuator. In: *2016 IEEE International Conference on Prognostics and Health Management (ICPHM)*, 1–8.
15. Karam W, Mare JC (2009) Modelling and simulation of mechanical transmission in roller screw electromechanical actuators. *Aircr Eng Aerosp Tec* 81: 288–298.
16. Leboeuf N, Nahid-Mobarakeh B, Takorabet N, et al. (2011) Modeling of PM Synchronous Machines Under Inter-turn Fault.
17. Leboeuf N, Boileau T, Nahid-Mobarakeh B, et al. (2012) On Inductance Calculations in PM Motors Under Fault Conditions. *IEEE T Magn* 48: 2605–2616.
18. Comon P (1994) Independent component analysis, A new concept? *Signal Process* 36: 287–314.
19. Comon P and De Lathauwer L (2010) Algebraic identification of under-determined mixtures. In: *Handbook of Blind Source Separation*, 325–365.
20. Moreau E and Comon P (2010) Contrasts. In: *Handbook of Blind Source Separation*, 65–105.
21. Hyvärinen A (1999) Fast and robust fixed-point algorithms for independent component analysis., *IEEE T Neural Network* 10: 626–634.
22. Hyvärinen A (2019) FastICA Matlab Package [Accessed: 30-Sept-2019]. Available from: http://research.ics.aalto.fi/ica/fastica/.

23. Torres ME, Colominas MA, Schlotthauer G, et al. (2011) A complete ensemble empirical mode decomposition with adaptive noise. *IEEE international conference on acoustics, speech and signal processing (ICASSP)*, 4144–4147.
24. Huang NE, Shen Z, Long SR, et al. (1998) The empirical mode decomposition and the Hilbert spectrum for nonlinear and non-stationary time series analysis. *Proceedings of the Royal Society of London A: Mathematical, Physical and Engineering Sciences* 454: 903–995.
25. Rao BKN (1996) Handbook of Condition Monitoring. 1st ed edition. Oxford, UK: Elsevier.
26. Kudo M and Sklansky J (2000) Comparison of algorithms that select features for pattern classifiers. *Pattern Recogn* 33: 25–41.

AIMS Press